01 Jan 1977

Surface Electromagnetic Waves with Damping. II. Anisotropic Media

G. S. Kovener

Ralph William Alexander
Missouri University of Science and Technology, ralexand@mst.edu

I. L. Tyler

Robert John Bell
Missouri University of Science and Technology

Recommended Citation

G. S. Kovener et al., "Surface Electromagnetic Waves with Damping. II. Anisotropic Media," *Physical Review B*, vol. 15, no. 12, pp. 5877 - 5882, American Physical Society, Jan 1977.
The definitive version is available at https://doi.org/10.1103/PhysRevB.15.5877

Surface electromagnetic waves with damping. II. Anisotropic media*

G. S. Kovener,† R. W. Alexander, Jr., I. L. Tyler, and R. J. Bell
Physics Department, University of Missouri-Rolla, Rolla, Missouri 65401
(Received 17 May 1976; revised manuscript received 9 March 1977)

The technique of plotting the attenuated-total-reflection (ATR) reflectance as a function of both frequency and incident angle using a three-dimensional plot is applied to surface electromagnetic waves (SEW) in a uniaxial material, MnF_2. It is shown that dispersion curves calculated without absorption do not completely describe the ATR reflectivity. Experimental data confirming the reflectance surface features are presented. Also, additional minima in the reflectance surface not associated with SEW are discussed.

I. INTRODUCTION

The three-dimensional ATR reflectance surface technique has been previously applied to isotropic materials in order to explain various aspects of the ATR spectra including the bend-back behavior of the surface electromagnetic wave (SEW) dispersion curves.[1,2] This technique of plotting reflectance as a function of both frequency and incident angle can be used for anisotropic materials, and we present a treatment of the attenuated total reflection (ATR) spectra for MnF_2, a uniaxial material, using the reflectance surface technique.

We have experimentally measured several branches of the SEW dispersion curves of MnF_2, and these results will be discussed. Several other features predicted by the reflectance surface approach to SEW have been confirmed experimentally.

II. THEORY

The description of SEW on anisotropic materials was first presented by Lyubimov and Sannikov[3] although surface magnetoplasmons which have a uniaxial dielectric tensor were treated earlier.[4-7] For nonmagnetic anisotropic materials, the first experimental observations of SEW using the ATR technique of Otto[8] were made by Bryksin, Mirlin, and Reshina[9,10] on MgF_2 and TiO_2, followed by Falge and Otto[11] on quartz, and by Perry, Fischer, and Buckel on CdS.[12]

Numerous articles have appeared discussing the theory of surface electromagnetic waves on uniaxial[3,4,6,10,13-17] and biaxial[18] media and recently a review article appeared.[19] Thus only a few pertinent results are summarized here. Otto and his co-workers have thoroughly discussed the uniaxial case for crystal quartz including experimental results.[11,20,21] Only three simple geometries were used for our measurements, namely; (I) the optic axis perpendicular to the surface (which is thus isotropic); (II) the optic axis parallel to the surface and k parallel to the optic axis; and (III) the optic axis parallel to the surface and k perpendicular to the optic axis. The x axis is taken along the direction of propagation and the z axis is the outward normal from the surface. The dispersion relations for the three cases are[3]

$$\text{case I: } k_x=(\omega/c)[(\epsilon_{\parallel}\epsilon_{\perp}-\epsilon_{\parallel})/(\epsilon_{\parallel}\epsilon_{\perp}-1)]^{1/2}, \tag{1a}$$

$$\text{case II: } k_x=(\omega/c)[(\epsilon_{\parallel}\epsilon_{\perp}-\epsilon_{\perp})/(\epsilon_{\parallel}\epsilon_{\perp}-1)]^{1/2}, \tag{1b}$$

$$\text{case III: } k_x=(\omega/c)[\epsilon_{\perp}/(\epsilon_{\perp}-1)]^{1/2}. \tag{1c}$$

The dielectric functions parallel and perpendicular to the optic axis are $\epsilon_{\parallel}$ and $\epsilon_{\perp}$, respectively. The dielectric functions were obtained from Ref. 22. The real parts of $\epsilon_{\parallel}$ and $\epsilon_{\perp}$ are plotted versus wave number in Fig. 1. The dispersion curves obtained from Eqs. (1) are plotted in Fig. 2. In plotting the dispersion curves the damping was set equal to zero, as is usually done. If damping is included, two problems arise. First, one must now take k_x or ω complex in Eqs. (1). If k_x is taken to be complex, the dispersion curves bend back, just as in the case of an isotropic crystal.[1,2] Although we have not attempted the solution of Eqs. (1) for ω complex and k_x real, there is no apparent reason for it to differ from the isotropic case[23] for which k_x approaches infinity as $\omega \to \omega_s$. Since Ref. 2 contains a detailed discussion of bend back, we will not consider it further.

A second problem with complex dielectric functions arises in connection with defining the existence of SEW. It is shown in Ref. 3 that existence of SEW require that $\epsilon_{\perp}(\omega)<0$ and $\epsilon_{\parallel}(\omega)\epsilon_{\perp}(\omega)>1$. This condition was obtained by requiring that the electromagnetic fields of the SEW decay exponentially normal to the surface in both directions. With complex dielectric constants, the fields always decay into the crystal and these conditions must be examined. Bryksin, Mirlin, and Reshina[10] proposed using just the real part of $\epsilon_{\parallel}(\omega)$ and $\epsilon_{\perp}(\omega)$ but this leads to inconsistencies in the assignment of SEW to minima in the ATR spectra.

This point is best illustrated by considering the

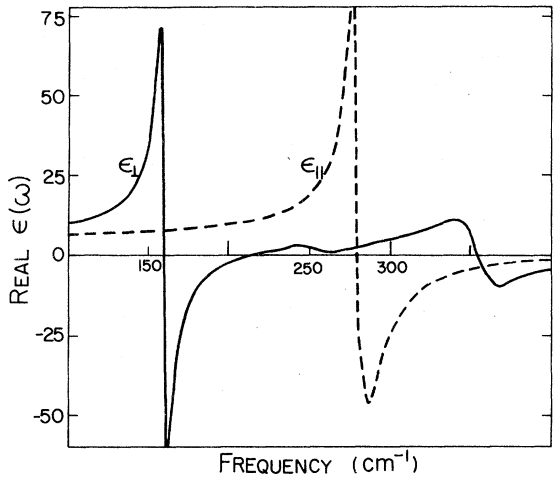

FIG. 1. Real part of the dielectric functions of MnF_2. The subscripts $\parallel$ and $\perp$ refer to the diagonal tensor components relative to the optic axis. Taken from Ref. 22.

dielectric function of MnF_2. Using the seven phonon model parameters for $\epsilon_\parallel(\omega)$ and the three phonon model parameters for $\epsilon_\perp(\omega)$ as given by Weaver *et al.*[22] the real part of $\epsilon(\omega)$ is plotted in Fig. 1. Note the small peak at 244 cm^{-1} in $\epsilon_\perp(\omega)$. This is due to a resonance at 254.1 cm^{-1}, but this oscillator strength is not sufficient to force the real part of $\epsilon_\perp(\omega)$ to be negative. Therefore no SEW should exist; yet, with no damping $\epsilon_\perp(\omega)$ (which is now real) is negative and a SEW should exist. An inconsistency is present at this frequency regarding the presence or absence of a SEW while, in fact, a minimum was observed in the experimental data near 258 cm^{-1} (case-I orientation). Thus Eqs. (1) are to be used with $\epsilon_\parallel(\omega)$ and $\epsilon_\perp(\omega)$ calculated with absorption neglected. As mentioned above this has been done in Fig. 2, where the dispersion branches for all three orientations are plotted in one graph. The solid lines are case I, the dash-dot lines are case II, and the dashed lines are case III. The arrows A indicate the maximum wave vector allowed for the extraordinary SEW as discussed below. For branch 2, the two cases I and III are not sufficiently different in frequency to be separated on this scale. Note that there is no case II extraordinary SEW until 280 cm^{-1}. The solid line labeled "light line" is the dispersion line of free-space photons, and the line labeled "silicon line" is the maximum wave vector available with a silicon ATR prism. Thus only one terminating branch, branch 1, would be accessible using a silicon prism. All three upper branches are asymptotic.

In Fig. 2 there are two branches which terminate for a finite value of the wave vector k. This termination occurs at the frequency and wave vector

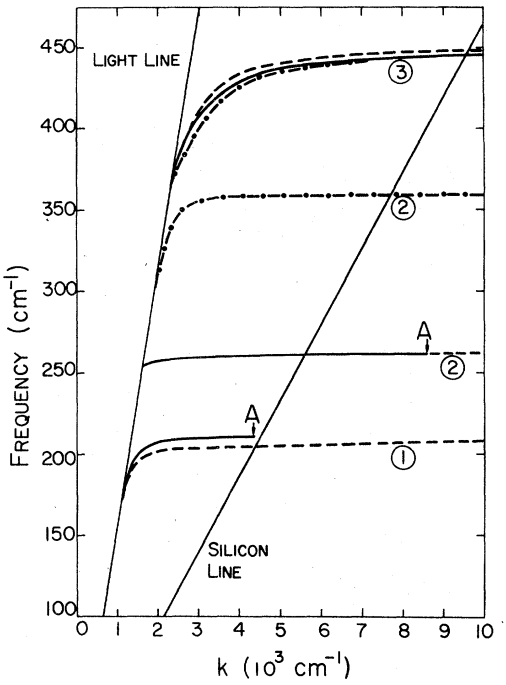

FIG. 2. Dispersion curves for MnF_2. The solid line is case I, the dash-dot line is case II, and the dashed line is case III. The arrows A indicate the termination points of the extraordinary SEW. The case-I and case-III curves are overlapping for the second branch on the scale. The line labeled "light line" is the free-space photon dispersion line, and the line labeled "silicon line" is the maximum momentum available with a silicon ATR prism.

where the surface electromagnetic wave dispersion curve crosses the longitudinal bulk optic phonon dispersion curve (which is flat). Thus, at the termination point the propagation vector is given by

$$k_T = (\omega_{lj}/c)[\epsilon_\parallel(\omega_{lj})]^{1/2}, \qquad (2)$$

where ω_{lj} is the longitudinal optic-phonon frequency of the jth oscillator of $\epsilon_\perp$.

III. EXPERIMENTAL

The ATR spectra of MnF_2 were measured using a RIIC FS-720 Michelson Fourier transform spectrometer with a Golay cell detector. The data were obtained by fixing the angle and "scanning" the frequency. In most cases, the apodized resolution was 2.0 cm^{-1}, and the uncertainty in the incident angle was ±2.0°. A sample holder for use with the RIIC TR-5 Micro ATR unit was fabricated to press the silicon ($n_p = 3.418$) hemicylinder prism against the crystal. The gap spacing was provided by Mylar spacers (2.0 μm), or if smaller gaps were required, the prism was pressed directly against the sample. The spacing was estimated using visi-

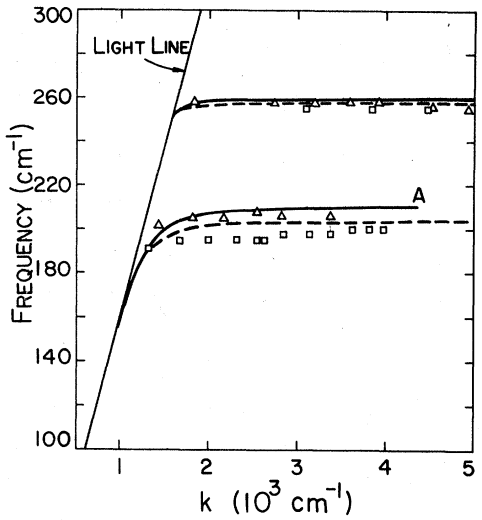

FIG. 3. Experimental dispersion curves for case I and case III. The solid line is the case-I dispersion curve and the dashed line is the case-III dispersion curve (see Fig. 2). The triangles are the experimental data points for the case-I configuration, and the squares are the data points for the case-III configuration. Point *A* is the theoretical termination point of the case-I extraordinary SEW.

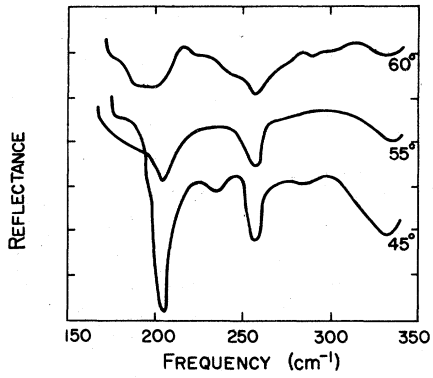

FIG. 4. Experimental ATR spectra showing a terminating branch. The orientation was case I, and the incident angles are as indicated. The gap was approximately 0.5 μm. The curves are offset for clarity. Note the abrupt disappearance of the lower frequency minimum, while the minimum at 258 cm^{-1} remains in the spectra at 60°.

ble-light interference fringes seen through the transparent MnF_2. The crystals were purchased from Optovac, Inc., and the surfaces were polished to $1/4\lambda$ (Na) flatness over a minimum of 80% of the surface. We have found that a large area must be flat in order to couple effectively (the incident beam diameter was approximately 5 mm). One face had the optic axis normal (basal face) and one face had the optic axis parallel to an edge (*CA* face). Since MnF_2 is a transparent uniaxial material, the orientation of the crystal is easily done with crossed polarizers. The beam divergence inside the prism was estimated to be 1.0°. All data were taken at room temperature.

The propagation vector of the surface electromagnetic wave k_x was determined from the frequency of the ATR minimum ω_{min} in the usual manner using

$$k_x = (\omega_{min}/c) n_p \sin\theta_{min}, \tag{3}$$

where n_p is the index of refraction of the prism. The results are plotted in Fig. 3. The triangles are the data points for case I and the squares for case III. The solid line is the case-I dispersion relation, and the dashed line is the case-III dispersion relation. The data for case III, branch 1, was taken with a 2.0-μm gap spacing while the gap spacing was 0.5 μm for the case-III branch-2 data. The data for case I was taken with a 0.5-μm gap. The experimental points are slightly lower in frequency than the theoretical values due to the use of finite gaps in the experiment. If one includes damping and the effects of the prism, both of which tend to lower the frequency of the observed minimum, good agreement is obtained with the measured dispersion curves. One of course includes damping and prism effects by calculating the ATR reflectivity using Fresnel's equations and plotting the minima in the reflectivity as the dispersion curve. Sohler has given Fresnel's equations for a layered system of anisotropic absorbing media.[24]

The higher-lying branches were not observed. The branch near 350 cm^{-1} is very weak while insufficient energy was available with our interferometer above 400 cm^{-1}. The termination of the extraordinary SEW at point *A* (for case I) was observed by noting the disappearance of branch 1 while branch 2 remained as the angle of incidence, and hence k_x, was increased. The experimental spectra are shown in Fig. 4. The minimum near 200 cm^{-1} disappears at about an angle of incidence of 60°. This angle is smaller than that predicted from Eq. (2), which gives an angle of 72°. Note, however, that other structure exists in the reflectivity in this region, which is discussed below.

Figures 5 and 6 show the calculated ATR reflectivity as a function of both the frequency of the incident radiation and the angle of incidence upon the prism base (for case I). The gap was 2 and 0.5 μm, respectively, for Figs. 5 and 6. If an experimental ATR spectra is measured by fixing the incident angle and scanning the frequency, the results will follow a cross section going from left to right. Conversely, if the ATR spectra is measured by fixing the frequency and scanning the incident angle, the results will follow a cross sec-

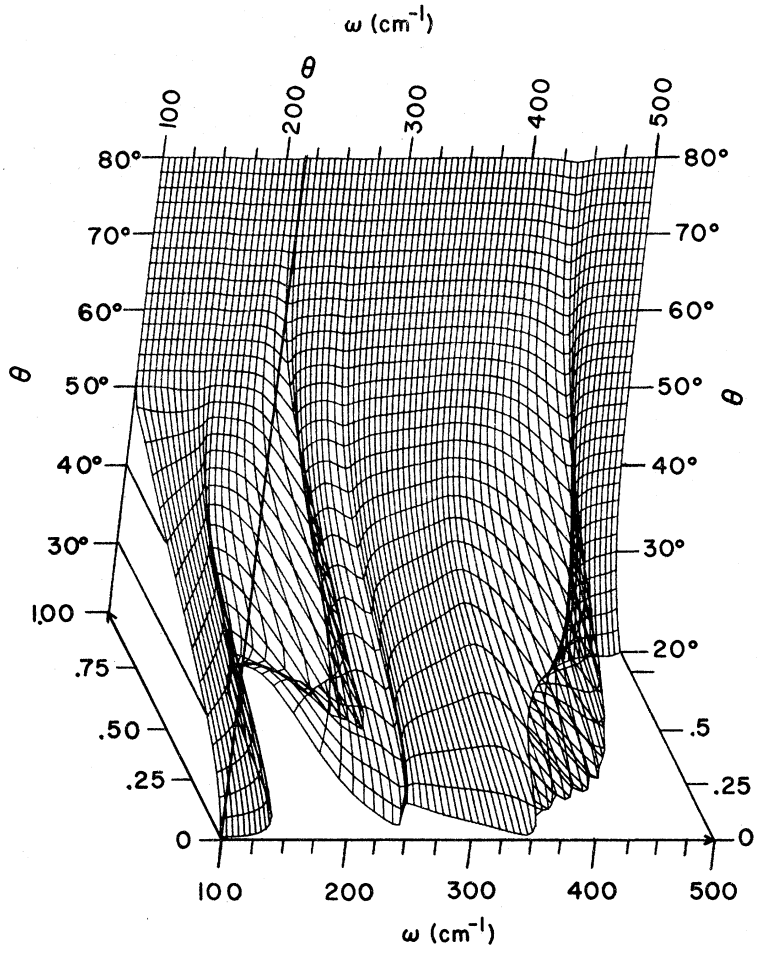

FIG. 5. Calculated ATR reflectance surface of case-I MnF_2. The reflectance is plotted in the vertical direction as a function of the frequency ω and the incident angle θ. The gap spacing is 2.0 μm. The frequency range is 100–500 cm^{-1}, and the incident angle is 20°–80°.

tion going from bottom to top. This is discussed further elsewhere.[1,2] Some general comments can be made. The dispersion of branch 3, for example, can be seen as the turning of the "valley" near 450 cm^{-1} toward lower ω as θ decreases. For a given ω, decreasing θ corresponds to decreasing k_x through the governing ATR equation

$$k_x = (\omega/c) n_p \sin(\theta), \tag{4}$$

where n_p is the prism index of refraction. For small angles of incidence, the reflectivity is small below 150 cm^{-1} because both $\epsilon_\perp$ and $\epsilon_\parallel$ are positive and considerable transmission occurs across the gap which is small compared to the wavelength. It is important to note that the low reflectivity is due to transmission across the gap into the MnF_2 crystal which is transparent in this frequency region and not due to absorption. At about 200 cm^{-1}, a valley can be seen, which for small angles of incidence (i.e., small values of k_x) turns "left" towards smaller ω. The bottom of this valley is the dispersion curve in Fig. 3 shown by the lower solid line. As seen in Fig. 6 (0.5-μm gap), considerable distortion of the dispersion curve has occurred because the presence of the prism is strongly felt by the surface electromagnetic wave.

The valleys of the branches of the dispersion curves near 250 and 400 cm^{-1} can also be seen. For the 0.5-μm gap one sees rather severe distortion for small angles of incidence, but it can be seen that if one wishes to look at large angles of incidence (and hence large k_x), that the smaller gap is required. Consider the 200-cm^{-1} branch which terminates. Equation (1) predicts a termination at an angle of incidence of 72°. The measured reflectivity for several angles of incidence are shown in Fig. 4 for a gap of 0.5 μm. The minimum near 200 cm^{-1} is very deep for an angle of incidence of 45°, but has essentially disappeared for an angle of incidence of 60°. Note that the minimum near 260 cm^{-1} becomes progressively weaker as the angle of incidence increases, but does not disappear. It, of course, is due to a nonterminating branch of the dispersion curve. It

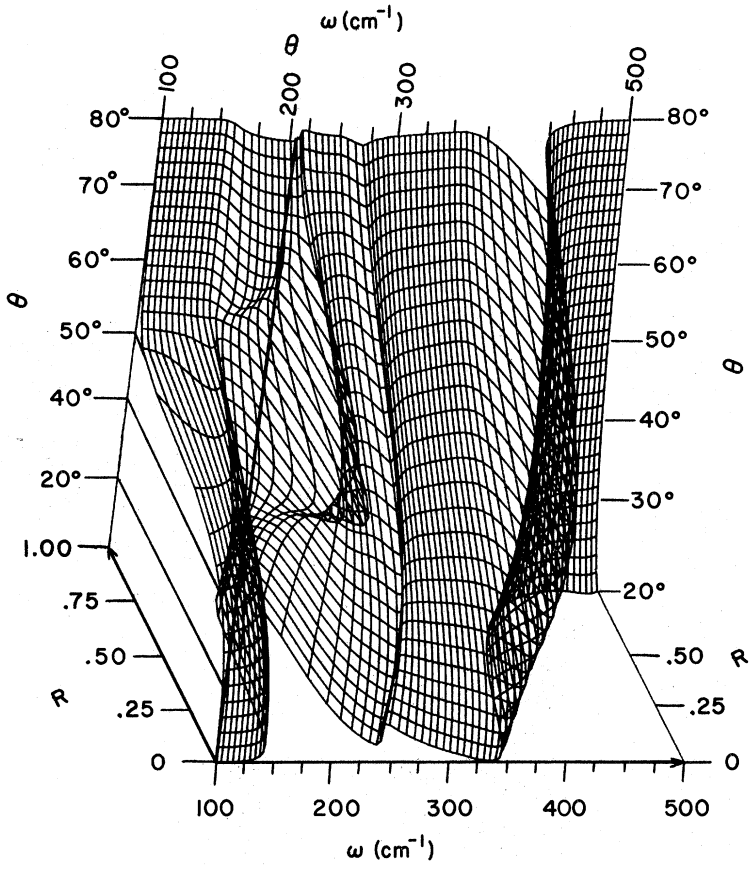

FIG. 6. Calculated ATR reflectance surface for case-I MnF_2. The gap spacing is 0.5 μm.

is difficult to determine exactly the angle of incidence at which the 200 cm^{-1} branch terminates because additional structure develops in the reflectivity at large angles of incidence. This is clearly seen in the calculated reflectivity (Fig. 6) where the terminating valley washes into a second valley for angles of incidence larger than about 60°. This second valley at large angles of incidence is not apparent at larger gaps (see Fig. 5), but the branch of the dispersion curve one wishes to measure is also very weak then. One can see a similar problem in the ATR spectra for terminating modes in crystal quartz,[18] although this problem was not discussed there. This second valley is due to the penetration of the incident radiation

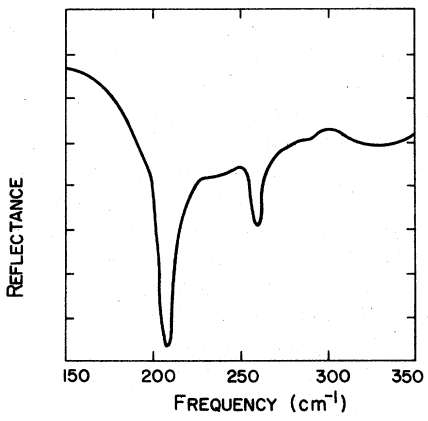

FIG. 7. Experimental ATR spectra of case-I MnF_2. The incident angle is fixed at 30°. The division along the ordinate are reflectance increments of 10%.

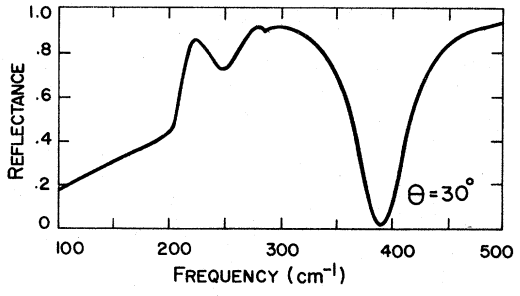

FIG. 8. Fixed-angle cross section of the reflectance surface for case-II orientation with a gap of 2.0 μm. The incident angle is 30°. The small dip at 280 cm^{-1} is the lowest frequency SEW predicted using the dispersion relation.

deeper into the MnF_2 crystal. That is, calculation shows that the imaginary part of k_z decreases in the valley region. Hence, one finds that the energy absorbed in the crystal increases so that the reflectivity decreases.

The branch seen just above 250 cm^{-1} is due to the weak oscillator 254 cm^{-1}, which was mentioned earlier. If damping is included, the real part of $\epsilon_\perp(\omega)$ is positive as shown in Fig. 2. Clearly however, this branch is observed in agreement with the dispersion curves calculated without damping. Figure 7 shows the measured ATR reflectance for an angle of incidence of 30°, showing observation of both the 200 and 250 cm^{-1} branches.

Figure 8 shows the calculated reflectance for case-II orientation for an angle of incidence of 30°. Note the pronounced minimum near 250 cm^{-1} and yet even with no damping, $\epsilon_\perp$ is positive in this region. The lowest predicted SEW branch for this orientation is near 280 cm^{-1} where a small dip in the reflectance can be seen. Our experimental measurements where not sufficiently good to see this minimum, although the other two were observed. What causes the dip near 250 cm^{-1}? In this region $\epsilon_\parallel(\omega)$ is becoming large so that the refractive index of MnF_2 is exceeding that of the silicon prism so that the total reflection is being frustrated in this frequency region. A calculation of the z component of the wave vector shows that, indeed, a propagating wave exists in the region of this reflectance minimum.

IV. CONCLUSION

The dispersion curves of surface electromagnetic waves (*TM* polarized) on MnF_2 have been measured for several branches using attenuated internal reflection. A three-dimensional plot of the ATR reflectivity is found to be a good method for interpreting the experimental data, particularly in understanding dips in the ATR reflectivity not caused by surface electromagnetic waves.

ACKNOWLEDGMENT

One of us (R.W.A.) would like to acknowledge a grant from the Research Corporation.

---

*Work supported by the NSF Grant No. DMR 75-19153.

†Present address: Amoco Chemical Corp., P.O. Box 400, Naperville, Ill. 60540.

[1]R. W. Alexander, G. S. Kovener, and R. J. Bell, Phys. Rev. Lett. 32, 154 (1974).

[2]G. S. Kovener, R. W. Alexander, Jr., I. L. Tyler, and R. J. Bell, Phys. Rev. B 14, 1458 (1976).

[3]V. N. Lyubimov and D. G. Sannikov, Fiz. Tverd. Tela 14, 675 (1972) [Sov. Phys.-Solid State 14, 575 (1972)]; and V. N. Lyubimov, Kristallogr. 17, 816 (1972) [Sov. Phys. Crystallogr. 17, 714 (1973)].

[4]K. W. Chiu and J. J. Quinn, Nuovo Cimento B 10, 1 (1972).

[5]E. D. Palik, R. Kaplan, R. W. Gammon, H. Kaplan, J. J. Quinn, and R. F. Wallis, Phys. Lett. A 45, 143 (1973).

[6]J. J. Brion, R. F. Wallis, A. Hartstein, and E. Burstein, Phys. Rev. Lett. 28, 1455 (1972).

[7]I. L. Tyler, B. Fischer, and R. J. Bell, Opt. Commun. 8, 145 (1973).

[8]A. Otto, Z. Phys. 216, 398 (1968).

[9]V. V. Bryksin, D. N. Mirlin, and I. I. Reshina, Pis'ma Zh. Eksp. Teor. Fiz. 16, 445 (1972) [JETP Lett. 16, 315 (1972)].

[10]V. V. Bryksin, D. N. Mirlin, and I. I. Reshina, Fiz. Tverd. Tela 15, 1118 (1972) [Sov. Phys.-Solid State 15, 760 (1973)].

[11]H. J. Falge and A. Otto, Phys. Status Solidi B 56, 523 (1973).

[12]C. H. Perry, B. Fischer, and W. Buckel, Solid State Commun. 13, 1261 (1973).

[13]A. Hartstein, E. Burstein, A. A. Maradudin, R. Brewer, and R. F. Wallis, J. Phys. C 6, 1266 (1973).

[14]O. A. Dubovskii, Fiz. Tverd. Tela 12, 3054 (1970) [Sov. Phys.-Solid State 12, 2471 (1971)].

[15]E. Schuller, G. Borstel, and H. J. Falge, Phys. Status Solidi B 69, 467 (1975).

[16]B. Fischer, D. Bauerle and W. J. Buckel, Solid State Commun. 14, 291 (1974).

[17]V. M. Agranovich, Usp. Fiz. Nauk 115, 199 (1975) [Sov. Phys. Usp. 18, 99 (1975)].

[18]G. Borstel, Phys. Status Solidi B 60, 427 (1973).

[19]G. Borstel, H. J. Falge, and A. Otto, in *Springer Tracts on Modern Physics*, edited by G. Höhler (Springer, Berlin, 1974), Vol. 74.

[20]H. J. Falge, A. Otto, and W. Sohler, Phys. Status Solidi B 63, 259 (1974).

[21]H. J. Falge, G. Borstel, and A. Otto, Phys. Status Solidi B 65, 123 (1974).

[22]J. H. Weaver, C. A. Ward, G. S. Kovener, and R. W. Alexander, J. Phys. Chem. Solids 35, 1625 (1974).

[23]R. W. Gammon and E. D. Palik, J. Opt. Soc. Am. 64, 350 (1974).

[24]W. Sohler, Opt. Commun. 10, 203 (1974).